Journal of Medicinal Chemistry

Article

pubs.acs.org/jmc

Structure−Efficiency Relationship of [1,2,4]Triazol-3-ylamines as Novel Nicotinamide Isosteres that Inhibit Tankyrases

Michael D. Shultz,* Dyuti Majumdar, Donovan N. Chin, Pascal D. Fortin, Yun Feng, Ty Gould, Christina A. Kirby, Travis Stams, Nigel J. Waters,† and Wenlin Shao

Novartis Institutes for Biomedical Research Incorporated, 250 Massachusetts Avenue, Cambridge, Massachusetts 02139, United States

Supporting Information

ABSTRACT: Tankyrases 1 and 2 are members of the poly(ADP-ribose) polymerase (PARP) family of enzymes that modulate Wnt pathway signaling. While amide- and lactam-based nicotinamide mimetics that inhibit tankyrase activity, such as XAV939, are well-known, herein we report the discovery and evaluation of a novel nicotinamide isostere that demonstrates selectivity over other PARP family members. We demonstrate the utilization of lipophilic efficiency-based structure−efficiency relationships (SER) to rapidly drive the evaluation of this series. These efforts led to a series of selective, cell-active compounds with solubility, physicochemical, and in vitro properties suitable for further optimization.

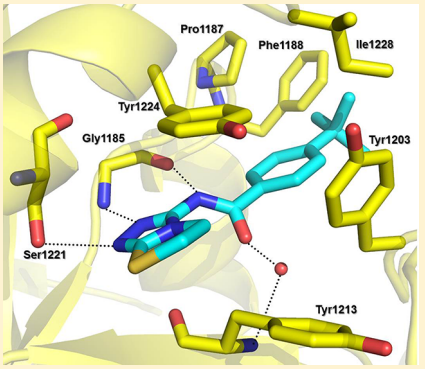

INTRODUCTION

Tankyrase (TNKS) 1 and 2, two members of the poly(ADP-ribose) polymerase (PARP) family, have been identified as potential targets for biochemical inhibition of the Wnt signaling pathway.[1] As such, recent efforts to develop low molecular weight inhibitors of these proteins have generated several new classes of Wnt pathway modulators.[2−6] The canonical pharmacophore for PARP inhibition is well-known and typically is achieved via nicotinamide isosteres such as lactams, pyridone, and pyrimidone motifs that bind in the nicotinamide binding pocket.[7] TNKS proteins appear to differ from other PARP family members by their ability to be inhibited by molecules that bind exclusively to the adenosine binding pocket.[5,8−11] The association of TNKS activity with a range of diseases such as cancer,[5,12−17] brain injury,[18] viral infections,[19] and pulmonary fibrosis[20] suggests TNKS as an attractive target for developing small-molecule antagonists. To this end, we engaged in efforts to identify a range of chemical scaffolds to validate TNKS inhibition as a modality for therapeutic intervention.

At the outset of hit finding efforts, we considered the requirements for compounds that would be required to validate TNKS as a cancer drug target.[21] Numerous attempts at target validation efforts have been confounded by the utilization of compounds with low selectivity for their intended target, where off-target activities led to erroneous conclusions regarding the disease dependency on the target in question. Since inhibition of other PARP family members are known to have anticancer activity, a pan-PARP inhibitor would not serve our initial purpose of target validation even though this could be a desirable clinical profile. It was also unclear at the outset whether the biology of the Wnt pathway and the potential advantages or limitations of targeting this pathway could be understood in the absence of an in vivo active compound. Therefore, we sought to rapidly develop an in vivo active compound with low off-target activity in order to evaluate which cancers may be dependent on TNKS activity. With these requirements in hand, we were motivated to explore hit prioritization and optimization approaches that would allow us to generate the desired profile in the most efficient manner possible.

The use of efficiency indices, also known as composite parameters, has been promoted as a way to more rapidly identify and advance quality chemical matter.[22,23] At the time we began this effort, high ligand efficiency (LE)[22] and lipophilic efficiency (LipE)[24] scores were used to rationalize high-quality hits and highly optimized compounds, respectively. To our knowledge, however, there was no study demonstrating the real-time use of a single composite parameter to enhance decision-making throughout the optimization process. The conventional wisdom is that LE should be used during early hit identification to maximize potency versus molecular size, and LipE should be used during later optimization stages to control for lipophilicity.[25] Since we had a variety of hits from our phenotypic cellular and high-throughput biochemical screens, in addition to structural and computational tools, we sought to focus on a single composite parameter to help simplify and accelerate the decision-making process from start to finish. We wondered if LipE could be utilized continuously from hit

Received: June 3, 2013

dx.doi.org/10.1021/jm400826j | J. Med. Chem. XXXX, XXX, XXX−XXX

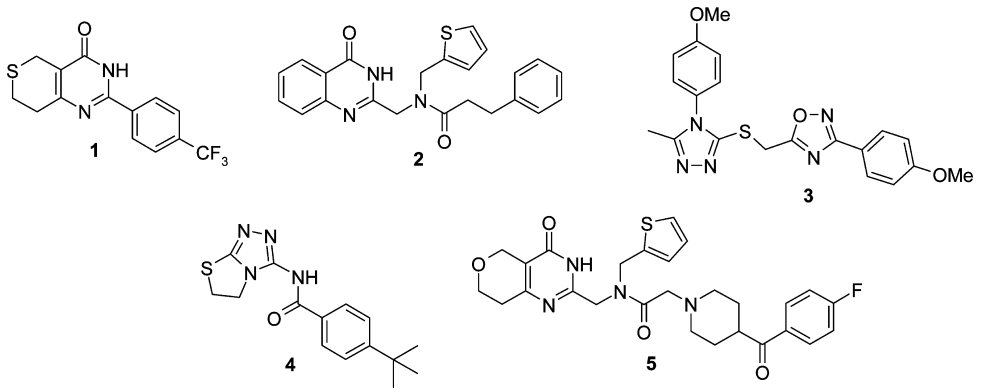

Figure 1. Early cellular phenotypic and biochemical high-throughput screening hits and partially optimized analogues used to generate pharmacophore model.

identification, through lead optimization, to candidate selection, and herein we report how this hypothesis was tested at the outset of identification and optimization of a novel series of tankyrase inhibitors.

RESULTS AND DISCUSSION

After a phenotypic cellular screen that identified XAV939[1] (**1**) as an antagonist of the Wnt pathway and tankyrase as the enzymatic target, we initiated a high-throughput screen (HTS) against tankyrase that identified multiple series, including novel adenosine pocket binders (compounds **2**–**4**, Figure 1).[26] Our phenotypic screen identified several distinct series of TNKS1/2 inhibitors, where structural biology efforts allowed us to generate multiple high-resolution crystal structures prior to completion of the HTS.[4,27,28] Multiple structures (**1**, **2**, and **5**) were aligned by the receptor structure by use of ICM.[29−31] We generated atomic property field (APF) values for the aligned ligands that formed the basis for the pharmacophore.[32] APFs are made up of three-dimensional property densities for several properties (hydrogen-bond donors/acceptors, hydrophobicity, and aromaticity). Each molecule has a set of APFs, and the overlay will result in higher density around regions of space with common field strength that can be visualized by a graphical view of the high-density contours (Figure S1 in Supporting Information), which constitutes the pharmacophore density that spans a wide range of binding modes. Upon completion of the HTS, interesting hits were docked into the pharmacophore model, and to our delight, several novel binding modes were identified, including compound **4** (Figure 2). This series has some of the highest LipE values identified from the HTS. We were very intrigued by this novel inhibitor of a PARP family member where the nicotinamide amide motif was replaced by an aminotriazole, which to our knowledge is a novel isostere of the nicotinamide moiety. The crystal structure of the catalytic domain of human TNKS1 complexed with compound **4** was determined to 2.3 Å resolution (PDB code 4KRS), and it revealed interactions that closely relate to those of the TNKS1/**1** complex.[28] These include a hydrogen bond between the triazole portion of **4** and the hydroxyl of Ser1221 as well as a hydrogen bond to the backbone amide of Gly1185 (Figure 3). The amide linker of **4** also forms a hydrogen bond to the carbonyl oxygen of Gly1185 and engages in a water-mediated hydrogen bond to the backbone amide of Tyr1213. Van der Waals interactions are maintained between **4** and both Tyr1213 and Tyr1224. The D-loop in the TNKS1/2 structure is ordered, adopting a similar conformation as reported in the

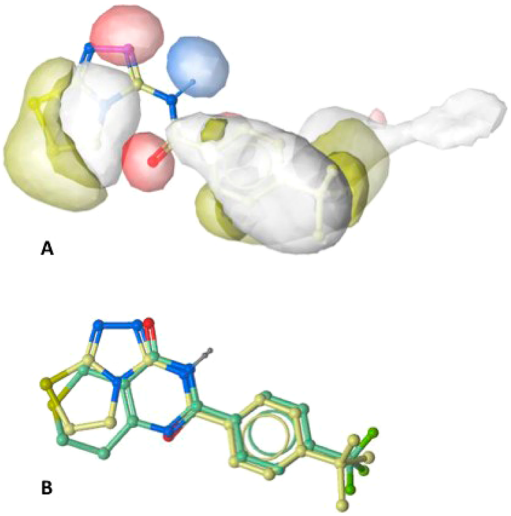

Figure 2. (A) Alignment of **4** with pharmacophore APF high density regions (red, hydrogen-bond acceptor; blue, hydrogen-bond donor; white, aromatic; yellow, hydrophobic). (B) Overlay of **4** with **1** based on pharmacophore model.

TNKS1/**1** complex structure,[28] with Tyr1203 making an edge−face stacking interaction with the phenyl ring of **4**. Additional van der Waals interactions exist between the *t*-butyl group of **4** and Pro1187, Phe1188, and Ile1228 of TNKS1. The solved structure was very similar to the structure predicted by our pharmacophore model (Figure S2 in Supporting Information)

Compound **4** was the most potent compound in this class identified by our screen, and traditional structure−activity relationship (SAR) studies revealed factors that modulated potency (Tables 1 and 3). We were curious if we could understand key interactions better and progress this series more rapidly by examining LipE-driven structure−*efficiency* relationships (SER) rather than potency-driven SAR. We sought to understand what maximized the efficiency of binding and utilized LipE in real time for decision-making. We include LE in this paper to highlight some interesting findings with this metric; however, LE was not utilized as a decision-making tool. One structural feature that substantially affects binding is the size of the thiazine ring (Table 1). As with compounds **4** and **6**, all molecular matched pairs (MMP) within this series demonstrated that five-membered rings were approximately 10-fold more potent and had improved LE/LipE relative to the corresponding six-membered rings. We observed that, with

dx.doi.org/10.1021/jm400826j | J. Med. Chem. XXXX, XXX, XXX−XXX

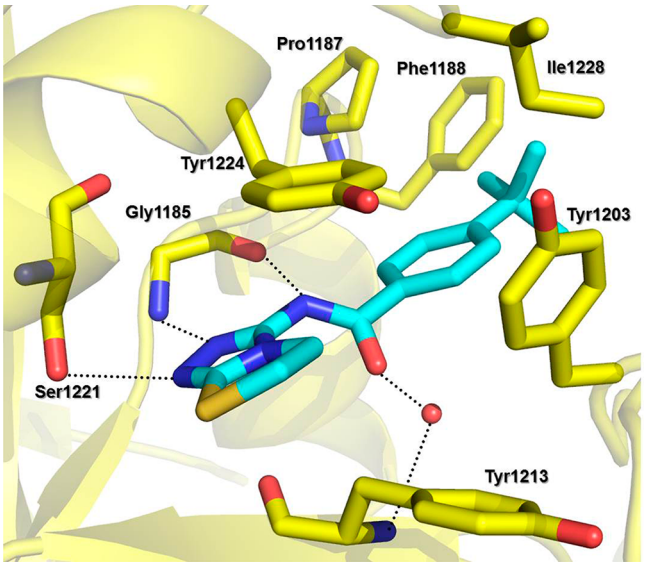

Figure 3. X-ray crystal structure of **4** in TNKS1 (PDB code 4KRS). Hydrogen bonds are shown as dashed lines. H-bond distances (clockwise from Ser1221, in angstroms) are 3.01, 2.87, 2.89, and 2.58 (**4** to H_2O) and 2.87 (H_2O to Tyr1213).

each MMP, the approximate 10-fold difference in potency from the removal of a methylene group (Δheavy atom count = +1, ΔclogP[33] = −0.2) led consistently to a ΔLipE of approximately +1.1, while for the lowest MW matched pair (**9** vs **10**) the LE improvement (0.13) was significantly greater than that of the highest MW matched pair (0.09 for **4** vs **6**). The LE dependence on MW has been noted elsewhere and illustrates how its use can be misleading.[34−36] It appears obvious that the five-membered ring is superior to the six-membered ring on the basis of potency. However, the SER tells us that although the 4-*tert*-butylphenyl amide is the most potent analogue within this series, it is also the least efficient, with compound **9** having an improved LipE (ΔLipE = +1.4) and LE (ΔLE = +0.16) relative to compound **4**. Further truncation of the alkyl amide (**11** and **12**) obliterated activity, and therefore further optimization was based on **9** due to the improved LipE and lower clogP despite being severalfold less potent than **4**. Analogues at this stage were spot-checked for activity against PARP1 and PARP2 and pathway inhibition. The PK profile of **9** in C57 BL/6 mice was determined (Table 2) and was characterized by low to moderate clearance and good oral bioavailability, and the C_{max} exceeded the cellular IC_{50} by 2-fold at a 5 mg/kg oral dose. The excellent in vitro safety profile (target hit rate of 0%, n = 122)[37,38] and high solubility coupled with the negative results versus hERG, Ames, and CYP450 panel suggests this novel series has excellent potential for further optimization.

We began investigating cycloalkyl amides (**13**−**16**, Table 3) by modification of 5,6-dihydrothiazolo[2,3-*c*][1,2,4]triazol-3-amine (Scheme 1) and found the cyclobutyl amide (**14**, LipE = 5.8) to have the most efficient ring size, while cyclohexyl (**16**) was the most potent of this subset. While the amplitude of SAR appeared substantial (ΔpIC_{50} = +1.5, approximately 30-fold range of potency) the SER amplitude was minimal (ΔLipE = +0.5, approximately 3-fold range of efficiency). Extending the ring further by a methylene (**17**) resulted in the first analogue in this series with submicromolar activity in the HEK293-STF reporter gene cellular assay. In this case potency was clearly improved and LE was slightly improved, but LipE was slightly reduced. The next two compounds highlight interesting aspects about SER-driven decision-making. Replacing the cyclohexyl moiety with a phenyl ring (**18**) or a tetrahydrofuran ring (**19**) reduces lipophilicity (ΔclogP of −1.2 and −2.4, respectively) such that an approximate 10-fold reduction in potency with **18** and **19** results in increased LipE of 0.1 and 1.4, respectively, but with a decrease in LE of 0.08 for both compounds. From a potency and LE perspective these two modifications are significantly less favorable, but from a LipE perspective **17** and **18** are similar while **19** is significantly more favorable than **17**.

Increasing the tether length by an additional methylene (**20**−**23**) provided the first single-digit nanomolar analogues in this series having similar biochemical activity as **1**. Analogues with longer alkyl chains (**24** and **25**) were 10-fold less active, suggesting an optimal tether length had already been achieved. A similar trend was observed where smaller cycloalkyl rings have more favorable potency, LipE, and LE (**20** and **21** vs **22**) while the phenyl ring (**23**), by virtue of its lower lipophilicity, was favored from a LipE perspective despite lower potency and LE than **21**. Modifications such as urea (**26**) and piperidine (**27**) demonstrated further dynamic SER. The lower LipE of **26** suggested that either conformational effects of the urea lowered affinity or the TNKS protein could not offer a polar interaction with the urea NH to compensate for the desolvation penalty introduced by this polar group. Compound **27** maintained constant LipE relative to **21** despite a 300-fold decrease in potency.

Despite a lower LE relative to **21**, compound **23** has higher LipE and therefore became our starting point for further analogue expansion (Table 4). While **19** had a more attractive LipE than **23**, we chose to sacrifice efficiency for the ability to generate analogues rapidly, with the assumption that the phenyl ring could be made more efficient by incorporating more efficient substituents and/or replacing with a heteroaryl motif. Our aim was to learn more about which types of interactions with TNKS were favored and improve the cellular activity of these compounds to the low nanomolar range. The low lipophilicity of **23** (clogP = 1.9) gave us the advantage of focusing on analogues with increased lipophilicity (**28**−**33**), a tactic that was well aligned with our goal for increasing cell potency. Halogen substituents at the ortho position (**28** and **29**) increased potency and LipE and, in the case of **29**, resulted in activity in the cellular assay that was slightly more potent than **1**, but they were less effective at other positions (data not shown). With a clogP of 2.6 and encouraging cell activity, compound **29** has improved physical chemical properties versus both **1** and **4** and a highly favorable LipE of 5.7. We undertook a brief examination of disubstituted aryl modifications to generate a tool compound that could be used to help us decide if this series had the potential for a successful lead optimization campaign.

The 2,6-dichloro analogue **30** resulted in lower LipE and slightly higher potency, while the lower activity of **31** clearly demonstrated the importance of at least one ortho chloro substituent. After intravenous administration in rats, **30** showed high CL (45.6 $mL \cdot min^{-1} \cdot kg^{-1}$) and a moderate volume of distribution (1.1 L/kg), in good agreement with the high in vitro microsomal clearance values. We examined additional dichloro analogues and found that the 2,3-dichlorophenyl moiety (**32**) was among the most efficient and cell-potent analogues in this series. This series demonstrates the dynamic SAR required for successful lead optimization; however,

dx.doi.org/10.1021/jm400826j | J. Med. Chem. XXXX, XXX, XXX−XXX

Table 1. Relationship between Thiazine Ring Size and Amide Substituents and Lipophilic and Ligand Efficiency[a]

Compound	Structure	TNKS2		IC_{50} (μM)				clogP
		LipE[a]	LE[b]	TNKS2	PARP1	PARP2	STF[c]	
1	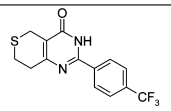	5.9 4.2[d]	0.55	0.0053	1.37	0.106	0.078	2.3 4.1[e]
4	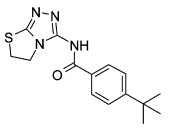	4.3	0.50	0.031	nd	>19	2.39	3.1
6	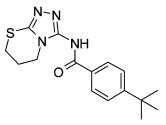	3.2	0.41	0.353	nd	>19	47.8	3.3
7	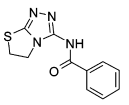	5.3	0.54	0.250	nd	nd	nd	1.3
8	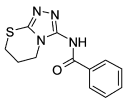	4.1	0.43	2.76	nd	nd	nd	1.5
9	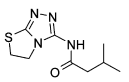	5.7	0.66	0.103	55.3	nd	6.45	1.3
10	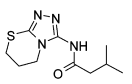	4.6	0.53	0.980	nd	nd	nd	1.4
11		-	-	>19 (9%)	nd	nd	nd	-0.2
12		-	-	>19 (5%)	nd	nd	nd	-0.02

[a]LipE = pIC_{50} (TNKS2) − clogP. [b]LE = 1.4pIC_{50}/(no.of heavy atoms). [c]HEK293 SuperTopFlash reporter gene assay. [d]LipE = pIC_{50} (TNKS2) − log *D*. [e]Measured log *D*. nd = not determined.

Table 2. Pharmacokinetic Profile of 9 in C57 BL/6 Mice[a]

	1 mg/kg iv dose	5 mg/kg po dose
AUC (nM·h)	4730	8595
AUC extrap (nM·h)	4747	8617
CL ($mL \cdot min^{-1} \cdot kg^{-1}$)	17	
V_{ss} (L/kg)	0.1	
$T_{1/2}$ (h)	0.1	
$T_{1/2}$ limits (h)	1−1	
T_{last} (h)	1	
MRT (0 − *t*) (h)	0.1	
C_{max} (nM)	19 074	13 679
T_{max} (h)	0.3	0.3
F (%)		36

[a]Following a single 1 mg/kg iv or 5 mg/kg po dose.

lipophilicity had increased significantly relative to compound **9** and further modifications to decrease lipophilicity were explored.

We next explored a heterocyclic subseries (**34**−**38**) based on compound **23** (Table 5). The most significant consequence of utilizing SER for decision-making is that one has to accept that modifications that reduce potency can be more favorable and should be retained in further rounds of analogue design. This point is illustrated with compounds **34**−**38**. In each case the heterocycle is less lipophilic than **23** so that it would be expected that if LipE were to remain constant, potency would necessarily decrease. For example, compounds **34** and **35** could be 30-fold less potent ($\Delta pIC_{50} = -1.5$) than **23** and maintain constant LipE since they are 30-fold less lipophilic (ΔclogP = −1.5). These compounds are only 3.5-fold less active than **25**, and thus their greater lipophilic efficiency (ΔLipE = 1) indicates the modifications exceeded expectations from a LipE perspective. While both the LipE and LE values are in highly attractive territory, it was believed that cellular activity needed to be improved. Combined with our earlier observation that polar functionality at this region improved LipE without enhancing potency,[39] we surmised that on this scaffold we were not orienting our heterocyclic substituents in a manner that

dx.doi.org/10.1021/jm400826j | J. Med. Chem. XXXX, XXX, XXX−XXX

Table 3. Variation of Ring Size and Tether Length and the Relationship with Lipophilic and Ligand Efficiency[a]

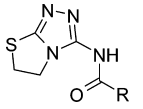

Compound	R	TNKS2		IC_{50} (μM)		clogP
		LipE[a]	LE[b]	TNKS2	STF[c]	
9		5.7	0.66	0.103	6.45	1.3
13		5.3	0.57	2.01	>50	0.40
14		5.8	0.61	0.264	13.8	0.73
15		5.4	0.58	0.220	12.8	1.3
16		5.4	0.59	0.070	1.54	1.8
17		5.2	0.60	0.020	0.429	2.5
18		5.3	0.52	0.239	7.27	1.3
19	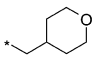	6.6	0.52	0.202	10.3	0.07
20	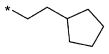	5.6	0.63	0.009	0.194	2.4
21	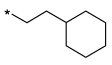	5.1	0.60	0.008	0.169	3.0
22	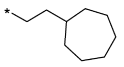	4.0	0.53	0.026	2.18	3.6
23	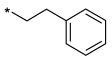	5.5	0.55	0.039	1.67	1.9
24	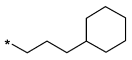	3.5	0.49	0.089	4.52	3.5
25	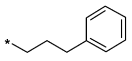	4.2	0.46	0.303	6.46	2.3
26	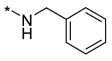	4.7	0.47	0.444	17.6	1.7
27	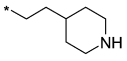	5.1	0.42	2.32	>50	0.58

[a]LipE = pIC_{50} (TNKS2) − clogP. [b]LE = $1.4pIC_{50}$/(no. of heavy atoms). [c]HEK293 SuperTopFlash reporter gene assay.

allowed productive or specific interactions with the TNKS binding pocket.

To further evaluate the ability of these compounds to modulate tankyrase function in a cellular context, the direct stabilization of Axin2 was measured in an ELISA format developed in-house. As the direct substrate for TNKS, Axin provided a proximal readout for cellular inhibition of TNKS1 and 2.[1] For multiple analogues, clear stabilization of Axin2 was

Scheme 1. General Synthetic Scheme for Preparation of Aminotriazole Analogues[a]

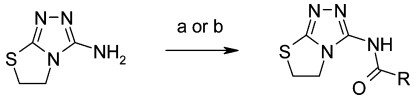

[a](a) RCOCl, DMAP, collidine. (b) RCOOH, EDCI, DMAP, Et_3N, THF.

Table 4. Structure–Efficiency Relationships of Mono- and Disubstituted Phenyl Rings[a]

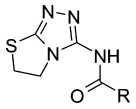

Compound	R	TNKS2		IC_{50} (μM)		clogP
		LipE[a]	LE[b]	TNKS2	STF[c]	
23		5.5	0.55	0.039	1.67	1.9
28		5.9	0.55	0.012	0.345	2.1
29		5.7	0.58	0.005	0.050	2.6
30		5.2	0.57	0.003	0.029	3.3
31		4.7	0.50	0.033	1.21	2.8
32	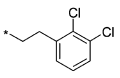	5.8	0.60	0.001	0.020	3.2
33	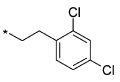	4.9	0.55	0.005	0.116	3.3

[a]LipE = pIC_{50} (TNKS2) − clogP. [b]LE = $1.4pIC_{50}$/(no. of heavy atoms). [c]HEK293 SuperTopFlash reporter gene assay.

detected, and in the case of **30**, submicromolar potency was achieved (Table 6). In contrast to other series,[4,39] the correlation between biochemical and cellular potency had some inconsistencies in this current series during the early stages of evaluation and optimization, but these diminished as on-target potency and efficiency improved. The most potent compounds had low solubility, which we speculate could contribute to the inconsistent cellular activity and highlights the importance of properties during hit series evaluation. Compound **30** lacks appreciable activity against PARP1/2 or other off targets; when tested against an internal panel of 120 safety targets, <50% inhibition at maximal concentration occurred for 118 panel members (target hit rate = 1.7%). We also evaluated the in vitro ADME properties, and in contrast to compound **9**, the more potent and lipophilic analogues in this series have significantly increased in vitro clearance in mouse liver microsomes. While rat and mouse liver microsomal stability data correlated well (data not shown), we observed significantly lower extraction ratios with human liver microsomes, suggesting the potential of species-dependent metabo-

dx.doi.org/10.1021/jm400826j | J. Med. Chem. XXXX, XXX, XXX–XXX

Table 5. Structure–Efficiency Relationships of Heterocyclic Analogues[a]

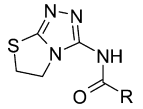

Compound	R	TNKS2 LipE[a]	TNKS2 LE[b]	IC_{50} (μM) TNKS2	IC_{50} (μM) STF[c]	clogP
23	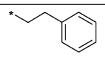	5.5	0.55	0.039	1.67	1.9
34	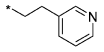	6.4	0.51	0.138	6.29	0.42
35	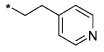	6.5	0.51	0.134	12.7	0.42
36		6.0	0.55	0.088	5.35	1.1
37		6.6	0.45	1.79	>10	-0.88
38	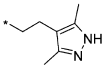	6.5	0.47	0.195	>10	0.22

[a]LipE = pIC_{50} (TNKS2) − clogP. [b]LE = 1.4pIC_{50}/(no. of heavy atoms). [c]HEK293 SuperTopFlash reporter gene assay.

lism (Table 6). Despite decreased microsomal stability and solubility activity, there was no significant erosion of the other favorable properties of compound **9** during our hit to lead optimization efforts, suggesting that SER may be effective for guiding decision-making early in the drug discovery process. Taken together, the data suggest potential for further optimization of this series, and the results of these efforts will be disclosed in due course.

Summary. Following our cell-based phenotypic screen for Wnt pathway antagonists, we initiated a biochemical HTS to enlarge the pool of available hits. A pharmacophore model was built prior to the confirmation of the HTS hits that allowed us to rapidly identify novel binding modes and interesting scaffolds to pursue. These efforts identified **4**, a highly efficient tankyrase inhibitor that represents a novel isostere of nicotinamide-based PARP inhibitors with substantial selectivity versus the other PARP family members tested. By utilizing structure–efficiency relationships to drive the optimization based on LipE rather than absolute potency, a novel class of highly potent and selective tankyrase inhibitors with highly favorable properties was generated. The combination of pharmacophore model, favorable properties, and LipE-driven optimization led to this series progressing into lead optimization only 4 months after **4** was confirmed as a hit. The use of LipE-based SER-driven decision-making facilitated this rapid evaluation and potency improvement without the identification of any new off-target liabilities.

MATERIALS AND METHODS

Tankyrase AutoPARsylation Assay. PARP catalytic activity was monitored by quantitative liquid chromatography/mass spectrometry (LC-MS) detection of nicotinamide, as previously described.[40] The autoPARsylation reactions were performed at room temperature in 384-well Greiner flat-bottom plates. The final reaction mixture contained 2.5% dimethyl sulfoxide (DMSO) and inhibitors with concentrations ranging from 0.0001 to 18.75 μM. GST-TNKS2P, GST-TNKS1P, PARP1, and PARP2 enzymes were used at final concentrations of 5, 5, 5, and 2 nM, respectively. The nicotinamide concentration in the resulting supernatants was measured by LC-MS. The percent inhibition was calculated as (control − sample)/(control − background) × 100. "Control" is the average value of eight wells without compound, and "background" is the average of eight wells mixed with 5× quenching solution and measured prior to initiation of the reaction.

SuperTopFlash Reporter Gene Assay. Compound activity in inhibiting Wnt ligand-induced signaling was measured by a Wnt-responsive SuperTopFlash (STF) luciferase reporter gene assay in HEK293 cells. The percent inhibition was calculated as (maximum Wnt-induced signaling − sample)/ (maximum Wnt-induced signaling − background) × 100. Maximum Wnt-induced signaling is the STF signal level induced by 20% Wnt3A CM without compound, and "background" is the STF signal level without the addition of Wnt3A CM or compound. To demonstrate the specific activity of inhibitors regulating Wnt signaling, a counterscreen was performed in HEK293T cells expressing a cAMP-response element (CRE) luciferase reporter gene. Compound activity on the CRE reporter was measured in the presence of 10 μM forskolin, which is an activator of cAMP signaling.

Axin2 Protein ELISA. Compound activity in stabilizing the Axin2 protein was measured by sandwich enzyme-linked immunosorbent (ELISA) assay in the colorectal cell line SW480. Cell lysates were prepared from cells treated with compounds in six-point dilution starting at 10 μM for 24 h. For the ELISA assay, anti-Axin2 capture antibody was diluted to a concentration of 1 μg/mL (1:1000) in carbonate coating buffer, pH 9.2 (Sigma, C3041-50CAP). Then 100 μL of the diluted anti-Axin2 capture antibody per well was used to coat the 96-well plate overnight at 4 °C. Plates were then washed three times with wash solution, PBST20 (phosphate-buffered saline, PBS, + 0.05% Tween), and blocked with 1% bovine serum albumin (BSA) in PBS for 1.5 h at room temperature while shaking gently. After blocking, plates were then washed three times with wash solution. Then 100 μL of prepared SW480 cell lysate was added to each well and incubated at room temperature for 2 h while being shaked gently. After washing, 100 μL of biotinylated anti-Axin2 antibody was added

Table 6. Cellular Axin2 Stabilization and in Vitro Metabolic Stability Data of Select Analogues

compd	IC_{50} (μM) TNKS1	TNKS2	PARP1	PARP2	axin2	mER[a]	hER[b]	clogP	solubility pH 6.8 (μM)
9	0.395	0.103	55.3	nd[c]	7.67	0.29	0.17	1.3	>1000
4	0.299	0.038	nd	>19	>10	0.84	0.36	3.1	>100
20	0.028	0.009	nd	nd	3.08	0.91	0.68	2.4	630
21	0.032	0.008	nd	nd	>10	0.95	0.20	3.0	520
29	0.014	0.005	nd	nd	1.40	0.90	0.66	2.6	32
30	0.012	0.003	>19	>19	0.377	0.91	0.61	3.3	16
32	0.007	0.001	>19	3.8	>10	0.92	nd	3.2	nd
33	0.024	0.006	>19	4.7	>10	0.91	nd	3.3	nd

[a]Mouse liver microsome extraction ratio. [b]Human liver microsome extraction ratio. [c]nd = not determined.

dx.doi.org/10.1021/jm400826j | J. Med. Chem. XXXX, XXX, XXX–XXX

to each well and the plates were incubated at room temperature for 2 h. Signal was detected by chemiluminescence (Pierce SuperSignal ELISA Femto, no. 3704) with streptavidin–horseradish peroxidase (HRP) (R&D Systems, DY998) and measured on Perkin-Elmer Wallac 1420 plate reader.

Protein Purification and Crystallization. Human TNKS1 protein was expressed, purified, and crystallized as previously described.[27] To obtain crystals containing **4**, TNKS1/PJ34 complex crystals were transferred into a soaking solution containing 100 mM Bis-tris, pH 5.8, 18% poly(theylene glycol) (PEG) 3350, 320 mM ammonium sulfate, and 200 μM **4**. Transfer of the crystals into fresh solution occurred once per hour over a 4-h period. Crystals were cryoprotected in the same soaking solution with the addition of 20% glycerol, followed by flash freezing directly into liquid nitrogen.

Data Collection and Structure Determination. Diffraction data for the TNKS1/**4** complex were collected on a Dectris Pilatus 6 M Detector at the Swiss Light Source beamline X06SA at a wavelength of 1 Å. The data were measured from a single crystal, and the reflections were indexed, integrated, and scaled by use of XDS and XSCALE.[34] The space group of the complex was *C*2 with two molecules in the asymmetric unit. The structure was determined by Fourier methods, with the TNKS1/PJ34 structure (PDB ID 3UH2) with active-site waters and inhibitors removed as the starting model.

Structure determination was achieved through iterative rounds of positional and simulated annealing refinement using PHENIX[35] with model building using COOT.[36] Individual *B*-factors were refined and a bulk solvent correction was applied. The solvent, sulfate ions, and inhibitor were built into the density in later rounds of the refinement. Data collection and refinement statistics are shown in Table 7.

Pharmacokinetic Analysis. All animal-related procedures were conducted under a Novartis IACUC-approved protocol in compliance with Animal Welfare Act regulations and the Guide for the Care and Use of Laboratory Animals.

Table 7. Crystallographic Data and Refinement Information

parameters	TNKS1/2 complex
space group	*C*2
a (Å)	124.6
b (Å)	44.2
c (Å)	87.8
α (deg)	90
β (deg)	90.1
γ (deg)	90
resolution range (Å)	43.92–2.29
total observations	68 241
unique reflections	21 041
completeness[a] (%)	97.9 (99.2)
I/σ[a]	12.5 (3.3)
R_{sym}[a,b]	0.064 (0.360)
R_{cryst}/R_{free}[c]	0.207/0.269
protein atoms	3330
heterogen atoms	198
solvent molecules	129
avg *B*-factor (Å^2)	
protein atoms	39.4
inhibitor atoms	35.8
rms deviations from ideal values	
bond lengths (Å)	0.008
bond angle (deg)	1.025

[a]Numbers in parentheses are for the highest resolution shell. [b]$R_{sym} = \sum|I_h - \langle I_h\rangle|/\sum I_h$ over all h, where I_h is the intensity of reflection h. [c]R_{cryst} and $R_{free} = \sum||F_o| - |F_c||/\sum|F_o|$, where F_o and F_c are observed and calculated amplitudes, respectively. R_{free} was calculated with 5% of data excluded from the refinement.

Rat Pharmacokinetic Studies. Intravenous PK studies were performed with male Sprague-Dawley rats weighing 220–270 g that are approximately 6–10 weeks old, obtained from Harlan Research Laboratories (South Easton, MA), each bearing dual implanted jugular vein cannulas. The intravenous dose for compound **20** was prepared at 0.2 mg/mL in a solution containing 10% PG and 90% PBS. Each animal received 1 mL of the solution/kg of body weight via intravenous injection into the jugular vein cannula.

Mouse Pharmacokinetic Studies. Mouse PK studies were performed with male C57BL/6 mice weighing 25–30 g that are approximately 6–8 weeks old, obtained from Harlan Research Laboratories (South Easton, MA). The intravenous dose for **9** was prepared at 0.2 mg/mL in a solution containing 10% PG and 90% PBS. Each animal received 1 mL of the solution/kg of body weight via intravenous injection into the lateral tail vein. The oral dose was prepared at 0.5 mg/mL in a solution in the same formulation as the iv dose. Each animal received 10 mL of the dosing solution/kg of body weight by oral gavage.

For both rat and mouse PK, approximately 50 μL of whole blood was collected from the tail of each animal by use of a microvette EDTA (ethylenediaminetetraacetic acid) tube, at 5 min (iv dose only) and (oral 0.25 only) 0.5, 1, 2, 4, and 7 h postdose and transferred to a EDTA tube. The blood was centrifuged at 3000 rpm and plasma was transferred to a PCR-96-AB-C 96-well plate, capped with PCR strip cap, and stored frozen (−20 °C) for parent compound analysis.

Measurement of Parent Compound. An LC-MS/MS method was used to detect **9** or **20** standards and in plasma. Nontreated C57BL/6 or Sprague-Dawley rat plasma was obtained from Bioreclamation, LLC. Compounds **9** and **20** as powder was dissolved in dimethyl sulfoxide to achieve the target free-base stock concentration of 1 mg/mL. Ten microliters of 1 mg/mL stock solution was spiked into 990 μL of nontreated C57BL/6 or Sprague-Dawley plasma. An automated serial dilution was performed with Tecan EVO 150 (Männedorf, Switzerland) to yield final plasma standard concentrations of 1, 5, 10, 50, 100, 500, 1000, and 5000 ng/mL. Aliquots (25 μL) of plasma treated with **9** or **20** and from the prepared standards and quality controls (QCs) were deproteinated by adding acetonitrile (150 μL) containing 50 ng/mL of the internal standard (IS; Glyburide). They were then vortex-mixed for 10 min and centrifuged for 5 min at 4 °C at 4000 rpm (2800*g*). An aliquot (125 μL) of the supernatant was transferred to a new plate, to which 50 μL of water was added. Then 10 μL of sample extract was injected for HPLC-MS/MS analyses. Chromatographic separation from interfering endogenous and exogenous contaminants was achieved on a MAC-MOD ACE C18 HPLC column (particle size 3 μm, column dimensions 2.0 × 30 mm) with 0.1% formic acid (FA) in water (A) and 0.1% FA in acetonitrile (B) as mobile-phase solvents and a linear gradient. The column oven temperature was set to 40 °C. The flow from the HPLC system (Shimazdu 20AD LC pump) was held at 700 μL·min^{-1} from 0 to 3.01 min. The flow was directly introduced into the ion source of a Sciex API4000 triple quadrupole (MS/MS) mass spectrometer (AB Sciex, Framingham, MA) and subjected to electrospray ionization (ESI, positive ion mode).

All pharmacokinetic (PK) parameters were derived from concentration–time data by noncompartmental analyses. All pharmacokinetic parameters were calculated with the computer program WinNonlin (Enterprise, Version 5.2) purchased from Pharsight Corp. (St. Louis, MO).

The peak concentrations (C_{max}) and times they occurred (T_{max}) were recorded. For the intravenous dose, the concentration of unchanged compound at time 0 in pharmacokinetics and excretion group was calculated from a log–linear regression of the first two data points to back-extrapolate $C(0)$. The area under the concentration–time curve (AUC_{last}) was calculated by use of the linear trapezoidal rule.

The total body clearance from the plasma (CL) and the apparent volume of distribution at steady state (V_{ss}) were calculated from the intravenous data, where AUC_{inf} and $AUMC_{inf}$ are the area under the concentration–time curve and area under the first moment concentration–time curve from time 0 to infinity, respectively.

dx.doi.org/10.1021/jm400826j | J. Med. Chem. XXXX, XXX, XXX–XXX

$$CL = \frac{dose_{iv}}{AUC_{inf}} V_{ss} = \frac{dose_{iv} AUMC_{inf}}{(AUC_{inf})^2}$$

AUC_{inf} was calculated from the following equation, where AUC_{last} was calculated by use of the linear trapezoidal rule:

$$AUC_{inf} = AUC_{last} + \frac{C_{last}}{\lambda_z}$$

The terminal elimination rate constant (λ_z) for the unchanged compound was the slope of the log linear line from at least the last three data points, and the half-life ($T_{1/2}$) was calculated. The bioavailability was estimated as follows (AUC_{last} was used if extrapolation was >20%):

$$\%F = \frac{AUC_{inf,po}}{AUC_{inf,iv}} \frac{dose_{iv}}{dose_{po}}$$

Results are expressed as mean. No further statistical analysis was performed.

Chemistry. All solvents employed were commercially available "anhydrous" grade, and reagents were used as received unless otherwise noted. A Biotage Initiator Sixty system was used for microwave heating. Flash column chromatography was performed on Analogix Intelliflash 280 using Si 50 columns (32−63 μm, 230−400 mesh, 60 Å). NMR spectra were recorded on a Bruker AV400 (Avance 400 MHz) or AV600 (Avance 600 MHz) instruments. Analytical LC-MS was conducted on an Agilent 1100 series with UV detection at 214 and 254 nm, and an electrospray mode (ESI) coupled with a Waters ZQ single quad mass detector. One of two methods was used: In method A, 5−95% acetonitrile (ACN)/H_2O with 5 mM ammonium formate was used with a 2 min run and 3 μL injection through an Inertsil C8 column, 3 cm × 5 mm × 3 μm. In method B, 20−95% ACN/H_2O with 10 mM ammonium formate was used with a 2 min run and 3 μL injection through an Inertsil C8 column, 3 cm × 5 mm × 3 μm. The purity of all compounds was determined by high-resolution (HR) HPLC/MS characterization and found to be >95% pure except as noted. HRMS data were recorded on a Waters LCT Premier mass spectrometer with dual electrospray ionization source and Agilent 1100 liquid chromatograph. The resolution of the MS system was approximately 12 000 [full width at half-maximum (fwhm) definition]. HPLC separation was performed at 1.0 mL/min flow rate with the gradient from 10% to 95% in 2.5 min. Ammonium formate (10 mM) was used as the modifier additive in the aqueous phase. Sulfadimethoxine (Sigma; protonated molecule m/z 311.0814) was used as a reference and acquired through the LockSpray channel every third scan. Examples **4**, **6**−**12**, and **18** were purchased from ChemDiv (http://us.chemdiv.com).

Syntheses. *5,6-Dihydrothiazolo[2,3-c][1,2,4]triazol-3-ylamine.* The title compound was prepared in accordance with a literature procedure.[36]

*N-(5,6-Dihydrothiazolo[2,3-c][1,2,4]triazol-3-yl)-cyclopropanecarboxamide (**13**): General Method A.* To an ice-cold suspension of 5,6-dihydrothiazolo[2,3-*c*][1,2,4]triazol-3-ylamine hydrobromide (150 mg, 0.672 mmol) in tetrahydrofuran (2 mL) were added 4-dimethylaminopyridine (41 mg, 0.34 mmol) and collidine (0.13 mL, 122 mg, 1.01 mmol). To this was added cyclopropanecarbonyl chloride (77 mg, 0.740 mmol) in tetrahydrofuran (1 mL), and the mixture was warmed up to ambient temperature and stirred for 16 h. The reaction was quenched with saturated aqueous ammonium chloride solution and extracted with dichloromethane. The extracts were dried (magnesium sulfate) and concentrated to an oil that was purified by silica gel column chromatography to give the title compound (44 mg, 0.209 mmol, 31% yield) as a white solid. ^{1}H NMR (400 MHz, CD_2Cl_2) δ 4.37 (t, J = 7.3 Hz, 2H), 3.94 (t, J = 7.0 Hz, 2H), 1.90−2.08 (m, 1H), 1.01−1.07 (m, 2H), 0.89−0.99 (m, 2H); MS m/z 211.1 (M + H); retention time 0.64 min; HRMS m/z (M + H) calcd for $C_8H_{10}N_4OS$ 211.0654, found 211.0648.

*N-(5,6-Dihydrothiazolo[2,3-c][1,2,4]triazol-3-yl)-cyclobutanecarboxamide (**14**): General Method B.* To a suspension of 3-(2-chlorophenyl)propanoic acid (74 mg, 0.740 mmol) and 5,6-dihydrothiazolo[2,3-*c*][1,2,4]triazol-3-ylamine hydrobromide (150 mg, 0.672 mmol) in *N*,*N*-dimethylformamide (3 mL) were added 1-ethyl-3-(3-dimethylaminopropyl)carbodiimide hydrochloride (193 mg, 1.01 mmol), *N*,*N*-dimethylaminopyridine (123 mg, 1.01 mmol), and triethylamine (0.24 mL, 177 mg, 1.75 mmol). The mixture was stirred at ambient temperature for 16 h and concentrated to an oil in vacuo. This was purified by silica gel column chromatography to give the title compound (135 mg, 0.542 mmol, 81% yield, 90% purity) as a white solid. ^{1}H NMR (400 MHz, CD_2Cl_2) δ 4.39 (t, J = 7.3 Hz, 2H), 3.96 (t, J = 7.3 Hz, 2H), 3.43 (quintet, J = 8.5 Hz, 1H), 2.23−2.41 (m, 4H), 2.00−2.13 (m, 1H), 1.83−1.99 (m, 1H); MS m/z 225.2 (M + H); retention time 0.79 min; HRMS m/z (M + H) calcd for $C_9H_{12}N_4OS$ 225.0810, found 225.0802.

*N-(5,6-Dihydrothiazolo[2,3-c][1,2,4]triazol-3-yl)-cyclopentanecarboxamide (**15**).* By general method A, 5,6-dihydrothiazolo[2,3-*c*][1,2,4]triazol-3-ylamine hydrobromide (150 mg, 0.672 mmol) and cyclopentanecarbonyl chloride (98 mg, 0.740 mmol) were converted to the title compound (110 mg, 0.462 mmol, 69% yield) as a white solid. ^{1}H NMR (400 MHz, CD_2Cl_2) δ 4.29−4.43 (m, 2H), 3.95 (t, J = 7.3 Hz, 2H), 3.00 (quintet, J = 7.9 Hz, 1H), 1.94−2.07 (m, 2H), 1.61−1.89 (m, 6H); MS m/z 239.2 (M + H); retention time 0.92 min; HRMS m/z (M + H) calcd for $C_{10}H_{14}N_4OS$ 239.0967, found 239.0963.

*N-(5,6-Dihydrothiazolo[2,3-c][1,2,4]triazol-3-yl)-cyclohexanecarboxamide (**16**).* By general method A, 5,6-dihydrothiazolo[2,3-*c*][1,2,4]triazol-3-ylamine hydrobromide (150 mg, 0.672 mmol) and cyclohexanecarbonyl chloride (99 mg, 0.672 mmol) were converted to the title compound (60 mg, 0.238 mmol, 35% yield) as a white solid. ^{1}H NMR (400 MHz, CD_2Cl_2) δ 4.34 (t, J = 7.0 Hz, 2H), 3.94 (t, J = 7.3 Hz, 2H), 2.45−2.58 (m, 1H), 1.95 (d, J = 12.6 Hz, 2H), 1.82 (td, J = 3.1, 12.4 Hz, 2H), 1.69−1.75 (m, 1H), 1.27−1.55 (m, 5H); MS m/z 253.2 (M + H); retention time 1.03 min; HRMS m/z (M + H) calcd for $C_{11}H_{16}N_4OS$ 253.1123, found 253.1124.

*2-Cyclohexyl-N-(5,6-dihydrothiazolo[2,3-c][1,2,4]triazol-3-yl)-acetamide (**17**).* By general method A, 5,6-dihydrothiazolo[2,3-*c*][1,2,4]triazol-3-ylamine hydrobromide (150 mg, 0.672 mmol) and cyclohexylacetyl chloride (119 mg, 0.740 mmol) were converted to the title compound (51 mg, 0.191 mmol, 28% yield) as a white solid. ^{1}H NMR (400 MHz, CD_2Cl_2) δ 4.37 (t, J = 7.3 Hz, 2H), 3.95 (t, J = 7.3 Hz, 2H), 2.39 (d, J = 7.0 Hz, 2H), 1.82−1.90 (m, 1H), 1.60−1.82 (m, 5H), 1.14−1.36 (m, 3H), 0.98−1.13 (m, 2H); MS m/z 267.4 (M + H); retention time 1.12 min; HRMS m/z (M + H) calcd for $C_{12}H_{18}N_4OS$ 267.1280, found 267.1283.

*N-(5,6-Dihydrothiazolo[2,3-c][1,2,4]triazol-3-yl)-2-(tetrahydropyran-4-yl)acetamide (**19**).* By general method A, 5,6-dihydrothiazolo[2,3-*c*][1,2,4]triazol-3-ylamine hydrobromide (150 mg, 0.672 mmol) and (tetrahydropyran-4-yl)acetyl chloride (120 mg, 0.740 mmol) were converted to the title compound (9 mg, 0.03 mmol, 5% yield) as a white solid. ^{1}H NMR (400 MHz, CD_3OD) δ 4.23 (t, J = 7.3 Hz, 2H), 4.05 (t, J = 7.0 Hz, 2H), 3.93 (dd, J = 3.8, 11.29 Hz, 2H), 3.37−3.50 (m, 2H), 2.36 (d, J = 7.5 Hz, 2H), 2.03−2.16 (m, 1H), 1.69 (d, J = 13.1 Hz, 2H), 1.27−1.45 (m, 2H); MS m/z 269.3 (M + H); retention time 0.99 min; HRMS m/z (M + H) calcd for $C_{11}H_{16}N_4O_2S$ 269.1072, found 269.1080.

*3-Cyclopentyl-N-(5,6-dihydrothiazolo[2,3-c][1,2,4]triazol-3-yl)-propionamide (**20**).* By general method A, 5,6-dihydrothiazolo[2,3-*c*][1,2,4]triazol-3-ylamine hydrobromide (150 mg, 0.672 mmol) and 3-cyclopentylpropionyl chloride (119 mg, 0.740 mmol) were converted to the title compound (96 mg, 0.36 mmol, 54% yield) as a white solid. ^{1}H NMR (400 MHz, CD_2Cl_2) δ 4.38 (t, J = 7.0 Hz, 2H), 3.95 (t, J = 7.3 Hz, 2H), 2.54 (t, J = 7.5 Hz, 2H), 1.82 (m, 3H), 1.72 (m, 2H), 1.65 (m, 2H), 1.55 (m, 2H); MS m/z 267.4 (M + H); retention time 1.17 min; HRMS m/z (M + H) calcd for $C_{12}H_{18}N_4O_6$ 267.1280, found 267.1284.

*3-Cyclohexyl-N-(5,6-dihydrothiazolo[2,3-c][1,2,4]triazol-3-yl)-propionamide (**21**).* By general method A, 5,6-dihydrothiazolo[2,3-*c*][1,2,4]triazol-3-yl-amine hydrobromide (100 mg, 0.448 mmol) and 3-cyclohexylpropionyl chloride (86 mg, 0.493 mmol) were converted to the title compound (87 mg, 0.310 mmol, 69% yield) as a white

dx.doi.org/10.1021/jm400826j | J. Med. Chem. XXXX, XXX, XXX−XXX

solid. ^{1}H NMR (400 MHz, CD_2Cl_2) δ 4.37 (t, J = 7.2 Hz, 2H), 3.95 (t, J = 7.2 Hz, 2H), 2.55 (t, J = 7.8 Hz, 2H), 1.53−1.82 (m, 7H), 1.10−1.39 (m, 4H), 0.84−1.02 (m, 2H); MS m/z 281.4 (M + H); retention time 1.26 min; HRMS m/z (M + H) calcd for $C_{13}H_{20}N_4OS$ 281.1436, found 281.1440.

*3-Cycloheptyl-N-(5,6-dihydrothiazolo[2,3-c][1,2,4]triazol-3-yl)-propionamide (**22**).* By general method B, 5,6-dihydrothiazolo[2,3-*c*][1,2,4]triazol-3-ylamine hydrobromide (150 mg, 0.672 mmol) and 3-cycloheptylpropionic acid (114 mg, 0.672 mmol) were converted to the title compound (135 mg, 0.459 mmol, 68% yield) as a white solid. ^{1}H NMR (400 MHz, CD_3OD) δ 4.22 (t, J = 7.0 Hz, 2H), 4.05 (t, J = 7.3 Hz, 2H), 2.42 (t, J = 7.5 Hz, 2H), 1.73−1.83 (m, 3H), 1.48−1.72 (m, 6H), 1.30−1.43 (m, 4H), 1.00−1.15 (m, 2H); MS m/z 295.3 (M + H); retention time 1.46 min; HRMS m/z (M + H) calcd for $C_{14}H_{22}N_4OS$ 295.1593, found 295.1602.

*N-(5,6-Dihydrothiazolo[2,3-c][1,2,4]triazol-3-yl)-3-phenylpropionamide (**23**).* By general method A, 5,6-dihydrothiazolo[2,3-*c*][1,2,4]-triazol-3-ylamine hydrobromide (150 mg, 0.672 mmol) and 3-phenylpropionyl chloride (119 mg, 0.706 mmol) were converted to the title compound (110 mg, 0.401 mmol, 60% yield) as a white solid. ^{1}H NMR (400 MHz, CD_2Cl_2) δ 7.11−7.36 (m, 5H), 4.21−4.35 (m, 2H), 3.93 (t, J = 7.0 Hz, 2H), 2.98−3.11 (m, 2H), 2.87 (t, J = 7.5 Hz, 2H); MS m/z 275.1 (M + H); retention time 1.11 min; HRMS m/z (M + H) calcd for $C_{13}H_{14}N_4OS$ 275.0967, found 275.0966.

*4-Cyclohexyl-N-(5,6-dihydrothiazolo[2,3-c][1,2,4]triazol-3-yl)-butanamide (**24**).* By general method B, 5,6-dihydrothiazolo[2,3-*c*][1,2,4]triazol-3-ylamine hydrobromide (150 mg, 0.672 mmol) and 4-cyclohexylbutyric acid (114 mg, 0.672 mmol) were converted to the title compound (98 mg, 0.333 mmol, 49% yield) as a white solid. ^{1}H NMR (400 MHz, DMSO-d_6) δ 10.84 (br s, 1H), 4.04−4.10 (m, 2H), 3.96−4.03 (m, 2H), 2.30 (t, J = 7.5 Hz, 2H), 1.50−1.72 (m, 7H), 1.10−1.27 (m, 6H), 0.78−0.93 (m, 2H); MS m/z 295.5 (M + H); retention time 1.40 min; HRMS m/z (M + H) calcd for $C_{14}H_{22}N_4OS$ 295.1593, found 295.1594.

*N-(5,6-Dihydrothiazolo[2,3-c][1,2,4]triazol-3-yl)-4-phenylbutanamide (**25**).* By general method A, 5,6-dihydrothiazolo[2,3-*c*][1,2,4]-triazol-3-ylamine hydrobromide (150 mg, 0.672 mmol) and 4-phenylbutanoyl chloride (123 mg, 0.672 mmol) were converted to the title compound (29 mg, 0.098 mmol, 15% yield) as a white solid. ^{1}H NMR (400 MHz, CD_2Cl_2) δ 7.12−7.36 (m, 5H), 4.38 (t, J = 7.3 Hz, 2H), 3.95 (t, J = 7.3 Hz, 2H), 2.66−2.76 (m, 2H), 2.59 (t, J = 7.5 Hz, 2H), 2.03 (quintet, J = 7.7 Hz, 2H); MS m/z 289.3 (M + H); retention time 1.29 min; HRMS m/z (M + H) calcd for $C_{14}H_{16}N_4OS$ 289.1123, found 289.1134.

*1-Benzyl-3-(5,6-dihydrothiazolo[2,3-c][1,2,4]triazol-3-yl)urea (**26**): General Method C.* To a solution of 5,6-dihydrothiazolo[2,3-*c*][1,2,4]triazol-3-ylamine hydrobromide (100 mg, 0. 450 mmol) in dimethylacetamide (1 mL) was added isocyanatomethylbenzene (95 mg, 0.717 mmol), and the mixture was subjected to microwave irradiation (120 °C for 15 min). The mixture was concentrated to an oil that was purified by silica gel column chromatography to give the title compound (37 mg, 0.134 mmol, 30% yield) as a white solid. ^{1}H NMR (400 MHz, DMSO-d_6) δ 9.85 (s, 1H), 8.16 (br s, 1H), 7.21−7.38 (m, 5H), 4.37 (d, J = 6.0 Hz, 2H), 4.06−4.15 (m, 2H), 3.96−4.05 (m, 2H); MS m/z 276.1 (M + H); retention time 1.06 min; HRMS m/z (M + H) calcd for $C_{12}H_{13}N_5OS$ 276.0919, found 276.0912.

4-[2-(5,6-Dihydrothiazolo[2,3-c][1,2,4]triazol-3-ylcarbamoyl)-ethyl]piperidine-1-carboxylic Acid tert-Butyl Ester: General Method D. To a suspension of 4-(2-carboxyethyl)piperidine-1-carboxylic acid *tert*-butyl ester (199 mg, 0.77 mmol) in tetrahydrofuran (3 mL) were added EDC (222 mg, 1.16 mmol), HOBt (178 mg, 1.16 mmol), and triethylamine (125 mg, 1.24 mmol). This misture was sonicated for a few minutes and 5,6-dihydrothiazolo[2,3-*c*][1,2,4]triazol-3-ylamine hydrobromide (121 mg, 0.85 mmol) was added. The mixture was stirred at ambient temperature for 16 h and then partitioned between ethyl acetate and saturated aqueous ammounium chloride solution. The aqueous layer was washed with more ethyl acetate and the combined organic extracts were dried over magnesium sulfate, filtered, and concentrated to an oil that was purified by silica gel column chromatography to give the title compound (78 mg, 0.20 mmol, 26% yield) as a white solid. ^{1}H NMR (400 MHz, CD_2Cl_2) δ 4.42−4.53 (m, 2H), 4.06 (br s, 2H), 3.98 (t, J = 7.3 Hz, 2H), 2.54−2.77 (m, 4H), 1.61−1.77 (m, 4H), 1.41−1.50 (m, 10H), 1.11 (dq, J = 4.3, 12.3 Hz, 2H); MS m/z 382.2 (M + H); retention time 1.35 min.

*N-(5,6-Dihydrothiazolo[2,3-c][1,2,4]triazol-3-yl)-3-piperidin-4-yl-propionamide Hydrochloride (**27**).* To a solution of 4-[2-(5,6-dihydrothiazolo[2,3-*c*][1,2,4]triazol-3-ylcarbamoyl)ethyl]piperidine-1-carboxylic acid *tert*-butyl ester (69 mg, 0.181 mL) in 1,4-dioxane/ethanol mixture (2 mL, 1:1, $^v/_v$) was added hydrogen chloride in 1,4-dioxane (0.27 mL, 4M, 1.09 mmol), and the mixture was stirred at ambient temperature for 24 h. The mixture was then concentrated to give the monohydrochloride salt of the title compound (60 mg, 0.179 mmol, 99% yield) as a white solid. ^{1}H NMR (400 MHz, CD_3OD) δ 4.46 (t, J = 7.3 Hz, 2H), 4.14 (t, J = 7.3 Hz, 2H), 3.40 (d, J = 13.1 Hz, 2H), 2.98 (t, J = 11.8 Hz, 2H), 2.66 (t, J = 7.3 Hz, 2H), 1.99 (d, J = 14.1 Hz, 2H), 1.67−1.78 (m, 3H), 1.35−1.51 (m, 2H); MS m/z 282.2 (M + H); retention time 0.97 min.

*N-(5,6-Dihydrothiazolo[2,3-c][1,2,4]triazol-3-yl)-3-(2-fluorophenyl)propionamide (**28**).* By general method D, 5,6-dihydrothiazolo[2,3-*c*][1,2,4]triazol-3-ylamine hydrobromide (150 mg, 0.672 mmol) and 3-(2-fluorophenyl)propionic acid (103 mg, 0.611 mmol) in tetrahydrofuran/*N*,*N*-dimethylformamide (3 mL, 2:1 v/v) were converted to the title compound (91 mg, 0.311 mmol, 51% yield) as a white solid. ^{1}H NMR (400 MHz, CD_2Cl_2) δ 7.32 (t, J = 7.5 Hz, 1H), 7.17−7.27 (m, 1H), 6.98−7.14 (m, 2H), 4.33 (t, J = 7.3 Hz, 2H), 3.94 (t, J = 7.3 Hz, 2H), 3.08 (t, J = 7.5 Hz, 2H), 2.86 (t, J = 7.5 Hz, 2H); MS m/z 293.1 (M + H); retention time 1.23 min; HRMS m/z (M + H) calcd for $C_{13}H_{13}FN_4OS$ 293.0872, found 293.0886.

*3-(2-Chlorophenyl)-N-(5,6-dihydrothiazolo[2,3-c][1,2,4]triazol-3-yl)propionamide (**29**).* By general method B, 5,6-dihydrothiazolo[2,3-*c*][1,2,4]triazol-3-ylamine hydrobromide (150 mg, 0.672 mmol) and 3-(2-chlorophenyl)propanoic acid (124 mg, 0.672 mmol) were converted to the title compound (180 mg, 0.583 mmol, 87% yield) as a white solid. ^{1}H NMR (400 MHz, CD_2Cl_2) δ 7.31−7.45 (m, 2H), 7.22 (dq, J = 5.8, 6.94 Hz, 2H), 4.22−4.38 (m, 2H), 3.94 (t, J = 7.3 Hz, 2H), 3.06−3.20 (m, 2H), 2.86 (t, J = 7.5 Hz, 2H); MS m/z 309.1 (M + H); retention time 1.19 min; HRMS m/z (M + H) calcd for $C_{13}H_{13}ClN_4OS$ 309.0577, found 309.0591.

*3-(2,6-Dichlorophenyl)-N-(5,6-dihydrothiazolo[2,3-c][1,2,4]-triazol-3-yl)propionamide (**30**).* By general method B, 5,6-dihydrothiazolo[2,3-*c*][1,2,4]triazol-3-ylamine hydrobromide (150 mg, 0.672 mmol) and 3-(2,6-dichlorophenyl)propionic acid (147 mg, 0.672 mmol) were converted to the title compound (198 mg, 0.577 mmol, 86% yield) as a white solid. ^{1}H NMR (400 MHz, DMSO-d_6) δ 11.06 (br s, 1H), 7.48 (d, J = 8.0 Hz, 2H), 7.30 (t, J = 8.0 Hz, 1H), 4.13 (t, J = 7.0 Hz, 2H), 4.01 (t, J = 7.3 Hz, 2H), 3.11−3.22 (m, 2H), 2.54−2.65 (m, 2H); MS m/z 343.1 (M + H); retention time 1.24 min; HRMS m/z (M +H) calcd for $C_{13}H_{12}Cl_2N_4OS$ 343.0187, found 343.0201.

*N-(5,6-Dihydrothiazolo[2,3-c][1,2,4]triazol-3-yl)-3-(2,6-dimethylphenyl)propionamide (**31**).* By general method B, 5,6-dihydrothiazolo[2,3-*c*][1,2,4]triazol-3-ylamine hydrobromide (100 mg, 0.448 mmol) and 3-(2,6-dimethylphenyl)propionic acid (80 mg, 0.448 mmol) were converted to the title compound (87 mg, 0.288 mmol, 64% yield) as a white solid. ^{1}H NMR (400 MHz, CD_3OD) δ 6.98 (s, 3H), 4.21 (t, J = 7.3 Hz, 2H), 4.05 (t, J = 7.3 Hz, 2H), 2.98−3.09 (m, 2H), 2.52−2.63 (m, 2H), 2.35 (s, 6H); MS m/z 303.2 (M + H); retention time 1.27 min; HRMS m/z (M + H) calcd for $C_{15}H_{18}N_4OS$ 303.1280, found 303.1286.

*3-(2,3-Dichlorophenyl)-N-(5,6-dihydrothiazolo[2,3-c][1,2,4]-triazol-3-yl)propionamide (**32**).* By general method B, 5,6-dihydrothiazolo[2,3-*c*][1,2,4]triazol-3-ylamine hydrobromide (100 mg, 0.448 mmol) and 3-(2,3-dichlorophenyl)propionic acid (98 mg, 0.448 mmol) were converted to the title compound (70 mg, 0.204 mmol, 45% yield) as a white solid. ^{1}H NMR (400 MHz, $CDCl_3$) δ 12.03 (br s, 1H), 7.31 (dd, J = 1.51, 8.0 Hz, 1H), 7.23 (dd, J = 1.5, 7.5 Hz, 1H), 7.10 (t, J = 7.8 Hz, 1H), 4.34 (t, J = 7.0 Hz, 2H), 3.91 (t, J = 7.3 Hz, 2H), 3.19 (t, J = 7.5 Hz, 2H), 2.88 (t, J = 7.5 Hz, 2H); MS m/z 343.0 (M + H); retention time 1.42 min; HRMS m/z (M + H) calcd for $C_{13}H_{12}Cl_2N_4OS$ 343.0187, found 343.0198.

dx.doi.org/10.1021/jm400826j | J. Med. Chem. XXXX, XXX, XXX−XXX

*3-(2,4-Dichlorophenyl)-N-(5,6-dihydrothiazolo[2,3-c][1,2,4]-triazol-3-yl)propionamide (**33**).* By general method B, 5,6-dihydrothiazolo[2,3-*c*][1,2,4]triazol-3-ylamine hydrobromide (150 mg, 0.672 mmol) and 3-(2,4-dichlorophenyl)propionic acid (147 mg, 0.672 mmol) were converted to the title compound (127 mg, 0.37 mmol, 55% yield) as a white solid. ^{1}H NMR (400 MHz, DMSO-d_6) δ 10.98 (br s, 1H), 7.61 (s, 1H), 7.33−7.43 (m, 2H), 3.94−4.10 (m, 4H), 2.91−3.04 (m, 2H), 2.68 (t, J = 7.3 Hz, 2H); MS m/z 343.4 (M + H); retention time 1.28 min; HRMS m/z (M + H) calcd for $C_{13n}H_{12}Cl_2N_4OS$ 343.0187, found 343.0202.

■ ASSOCIATED CONTENT

Ⓢ Supporting Information

Two figures, showing aligned ligands used for generation of pharmacophore and comparison of predicted and experimentally determined binding mode of **4**, and one table, listing safety profiling results of **4** and **30**. This material is available free of charge via the Internet at http://pubs.acs.org.

■ AUTHOR INFORMATION

Corresponding Author

*E-mail michael.shultz@novartis.com.

Present Address

†N.J.W.: Epizyme, 400 Technology Square, Cambridge, Massachusetts 02139, United States.

Author Contributions

The manuscript was written through contributions of all authors. All authors have given approval to the final version of the manuscript.

Notes

The authors declare no competing financial interest.

■ ACKNOWLEDGMENTS

We acknowledge the work of James Groarke and Guoping Xiao for protein purification of TNKS1. The TNKS data collection was performed on the X06SA beamline at the Swiss Light Source, Paul Scherrer Institut, Villigen, Switzerland.

■ ABBREVIATIONS USED

ADME, absorption distribution metabolism and excretion; APF, atomic property field; CYP450, cytochrome P450; CL, clearance; ELISA, enzyme-linked immunosorbent assay; HTS, high-throughput screen; LE, ligand efficiency; LipE, lipophilic efficiency; MMP, matched molecular pair; MW, molecular weight; PARP, poly(ADP-ribose) polymerase; PK, pharmacokinetic; SAR, structure−activity relationship; SER, structure−efficiency relationship; STF, SuperTopFlash; TNKS, tankyrase

■ REFERENCES

(1) Huang, S. M.; Mishina, Y. M.; Liu, S.; Cheung, A.; Stegmeier, F.; Michaud, G. A.; Charlat, O.; Wiellette, E.; Zhang, Y.; Wiessner, S.; Hild, M.; Shi, X.; Wilson, C. J.; Mickanin, C.; Myer, V.; Fazal, A.; Tomlinson, R.; Serluca, F.; Shao, W.; Cheng, H.; Shultz, M.; Rau, C.; Schirle, M.; Schlegl, J.; Ghidelli, S.; Fawell, S.; Lu, C.; Curtis, D.; Kirschner, M. W.; Lengauer, C.; Finan, P. M.; Tallarico, J. A.; Bouwmeester, T.; Porter, J. A.; Bauer, A.; Cong, F. Tankyrase inhibition stabilizes axin and antagonizes Wnt signalling. *Nature* **2009**, *461*, 614−620.

(2) Riffell, J. L.; Lord, C. J.; Ashworth, A. Tankyrase-targeted therapeutics: expanding opportunities in the PARP family. *Nat. Rev. Drug Discovery* **2012**, *11*, 923−936.

(3) Lu, J.; Ma, Z.; Hsieh, J. C.; Fan, C. W.; Chen, B.; Longgood, J. C.; Williams, N. S.; Amatruda, J. F.; Lum, L.; Chen, C. Structure-activity relationship studies of small-molecule inhibitors of Wnt response. *Bioorg. Med. Chem. Lett.* **2009**, *19*, 3825−3827.

(4) Shultz, M. D.; Kirby, C. A.; Stams, T.; Chin, D. N.; Blank, J.; Charlat, O.; Cheng, H.; Cheung, A.; Cong, F.; Feng, Y.; Fortin, P. D.; Hood, T.; Tyagi, V.; Xu, M.; Zhang, B.; Shao, W. [1,2,4]Triazol-3-ylsulfanylmethyl)-3-phenyl-[1,2,4]oxadiazoles: Antagonists of the Wnt pathway that inhibit tankyrases 1 and 2 via novel adenosine pocket binding. *J. Med. Chem.* **2012**, *55*, 1127−1136.

(5) Waaler, J.; Machon, O.; Tumova, L.; Dinh, H.; Korinek, V.; Wilson, S. R.; Paulsen, J. E.; Pedersen, N. M.; Eide, T. J.; Machonova, O.; Gradl, D.; Voronkov, A.; von Kries, J. P.; Krauss, S. A novel tankyrase inhibitor decreases canonical Wnt signaling in colon carcinoma cells and reduces tumor growth in conditional APC mutant mice. *Cancer Res.* **2012**, *72*, 2822−2832.

(6) Waaler, J.; Machon, O.; von Kries, J. P.; Wilson, S. R.; Lundenes, E.; Wedlich, D.; Gradl, D.; Paulsen, J. E.; Machonova, O.; Dembinski, J. L.; Dinh, H.; Krauss, S. Novel synthetic antagonists of canonical Wnt signaling inhibit colorectal cancer cell growth. *Cancer Res.* **2011**, *71*, 197−205.

(7) Woon, E. C.; Threadgill, M. D. Poly(ADP-ribose)polymerase inhibition: Where now? *Curr. Med. Chem.* **2005**, *12*, 2373−2392.

(8) Gunaydin, H.; Gu, Y.; Huang, X. Novel binding mode of a potent and selective tankyrase inhibitor. *PLoS One* **2012**, *7*, No. e33740.

(9) James, R. G.; Davidson, K. C.; Bosch, K. A.; Biechele, T. L.; Robin, N. C.; Taylor, R. J.; Major, M. B.; Camp, N. D.; Fowler, K.; Martins, T. J.; Moon, R. T. WIKI4, a novel inhibitor of tankyrase and Wnt/ss-catenin signaling. *PLoS One* **2012**, *7*, No. e50457.

(10) Narwal, M.; Venkannagari, H.; Lehtio, L. Structural basis of selective inhibition of human tankyrases. *J. Med. Chem.* **2012**, *55*, 1360−1367.

(11) Wahlberg, E.; Karlberg, T.; Kouznetsova, E.; Markova, N.; Macchiarulo, A.; Thorsell, A. G.; Pol, E.; Frostell, A.; Ekblad, T.; Oncu, D.; Kull, B.; Robertson, G. M.; Pellicciari, R.; Schuler, H.; Weigelt, J. Family-wide chemical profiling and structural analysis of PARP and tankyrase inhibitors. *Nat. Biotechnol.* **2012**, *30*, 283−288.

(12) Casas-Selves, M.; Kim, J.; Zhang, Z.; Helfrich, B. A.; Gao, D.; Porter, C. C.; Scarborough, H. A.; Bunn, P. A., Jr.; Chan, D. C.; Tan, A. C.; DeGregori, J. Tankyrase and the canonical Wnt pathway protect lung cancer cells from EGFR inhibition. *Cancer Res.* **2012**, *72*, 4154−4164.

(13) Gao, J.; Zhang, J.; Long, Y.; Tian, Y.; Lu, X. Expression of tankyrase 1 in gastric cancer and its correlation with telomerase activity. *Pathol. Oncol. Res.* **2011**, *17*, 685−690.

(14) Gelmini, S.; Poggesi, M.; Pinzani, P.; Mannurita, S. C.; Cianchi, F.; Valanzano, R.; Orlando, C. Distribution of t.ankyrase-1 mRNA expression in colon cancer and its prospective correlation with progression stage. *Oncol. Rep.* **2006**, *16*, 1261−1266.

(15) Gelmini, S.; Poggesi, M.; Distante, V.; Bianchi, S.; Simi, L.; Luconi, M.; Raggi, C. C.; Cataliotti, L.; Pazzagli, M.; Orlando, C. Tankyrase, a positive regulator of telomere elongation, is over expressed in human breast cancer. *Cancer Lett.* **2004**, *216*, 81−87.

(16) Seimiya, H.; Muramatsu, Y.; Ohishi, T.; Tsuruo, T. Tankyrase 1 as a target for telomere-directed molecular cancer therapeutics. *Cancer Cell* **2005**, *7*, 25−37.

(17) Seimiya, H. The telomeric PARP, tankyrases, as targets for cancer therapy. *Br. J. Cancer* **2006**, *94*, 341−345.

(18) Fancy, S. P. J.; Harrington, E. P.; Yuen, T. J.; Silbereis, J. C.; Zhao, C.; Baranzini, S. E.; Bruce, C. C.; Otero, J. J.; Huang, E. J.; Nusse, R.; Franklin, R. J. M.; Rowitch, D. H. Axin2 as regulatory and therapeutic target in newborn brain injury and remyelination. *Nat Neurosci.* **2011**, *14*, 1009−1016.

(19) Li, Z.; Yamauchi, Y.; Kamakura, M.; Murayama, T.; Goshima, F.; Kimura, H.; Nishiyama, Y. Herpes simplex virus requires poly(ADP-ribose) polymerase activity for efficient replication and induces extracellular signal-related kinase-dependent phosphorylation and ICP0-dependent nuclear localization of tankyrase 1. *J. Virol.* **2012**, *86*, 492−503.

(20) Ulsamer, A.; Wei, Y.; Kim, K. K.; Tan, K.; Wheeler, S.; Xi, Y.; Thies, R. S.; Chapman, H. A. Axin pathway activity regulates in vivo

pY654-beta-catenin accumulation and pulmonary fibrosis. *J. Biol. Chem.* **2012**, *287*, 5164−5172.
(21) Benson, J. D.; Chen, Y. N.; Cornell-Kennon, S. A.; Dorsch, M.; Kim, S.; Leszczyniecka, M.; Sellers, W. R.; Lengauer, C. Validating cancer drug targets. *Nature* **2006**, *441*, 451−456.
(22) Hopkins, A. L.; Groom, C. R.; Alex, A. Ligand efficiency: a useful metric for lead selection. *Drug Discovery Today* **2004**, *9*, 430−431.
(23) Abad-Zapatero, C.; Metz, J. T. Ligand efficiency indices as guideposts for drug discovery. *Drug Discovery Today* **2005**, *10*, 464−469.
(24) Leeson, P. D.; Springthorpe, B. The influence of drug-like concepts on decision-making in medicinal chemistry. *Nat. Rev. Drug Discov.* **2007**, *6*, 881−890.
(25) http://practicalfragments.blogspot.com/
(26) Shultz, M. D.; Kirby, C. A.; Stams, T.; Chin, D. N.; Blank, J.; Charlat, O.; Cheng, H.; Cheung, A.; Cong, F.; Feng, Y.; Fortin, P. D.; Hood, T.; Tyagi, V.; Xu, M.; Zhang, B.; Shao, W. [1,2,4]Triazol-3-ylsulfanylmethyl)-3-phenyl-[1,2,4]oxadiazoles: antagonists of the Wnt pathway that inhibit tankyrases 1 and 2 via novel adenosine pocket binding. *J. Med. Chem.* **2012**, *55*, 1127−1136.
(27) Kirby, C. A.; Cheung, A.; Fazal, A.; Shultz, M. D.; Stams, T. Structure of human tankyrase 1 in complex with small-molecule inhibitors PJ34 and XAV939. *Acta Crystallogr., Sect. F: Struct. Biol. Cryst. Commun.* **2012**, *68*, 115−118.
(28) Manuscript submitted for publication.
(29) Abagyan, R.; Totrov, M.; Kuznetsov, D. Icm, a new method for protein modeling and design: Applications to docking and structure prediction from the distorted native conformation. *J. Comput. Chem.* **1994**, *15*, 488−506.
(30) Abagyan, R.; Totrov, M. Biased probability Monte-Carlo conformational searches and electrostatic calculations for peptides and proteins. *J. Mol. Biol.* **1994**, *235*, 983−1002.
(31) Abagyan, R.; Orry, A.; Raush, E.; Budagyan, L.; Totrov, M. ICM Manual 3.5, 2011.
(32) Totrov, M. Atomic property fields: Generalized 3D pharmacophoric potential for automated ligand superposition, pharmacophore elucidation and 3D QSAR. *Chem. Biol. Drug Des.* **2008**, *71*, 15−27.
(33) Ertl, P.; Muhlbacher, J.; Rohde, B.; Selzer, P. Web-based cheminformatics and molecular property prediction tools supporting drug design and development at novartis. *SAR QSAR Environ. Res.* **2003**, *14*, 321−328.
(34) Nissink, J. W. Simple size-independent measure of ligand efficiency. *J. Chem. Inf. Model.* **2009**, *49*, 1617−1622.
(35) Reynolds, C. H.; Tounge, B. A.; Bembenek, S. D. Ligand binding efficiency: Trends, physical basis, and implications. *J. Med. Chem.* **2008**, *51*, 2432−2438.
(36) Reynolds, C. H.; Bembenek, S. D.; Tounge, B. A. The role of molecular size in ligand efficiency. *Bioorg. Med. Chem. Lett.* **2007**, *17*, 4258−4261.
(37) Lounkine, E.; Keiser, M. J.; Whitebread, S.; Mikhailov, D.; Hamon, J.; Jenkins, J. L.; Lavan, P.; Weber, E.; Doak, A. K.; Cote, S.; Shoichet, B. K.; Urban, L. Large-scale prediction and testing of drug activity on side-effect targets. *Nature* **2012**, *486*, 361−367.
(38) Bowes, J.; Brown, A. J.; Hamon, J.; Jarolimek, W.; Sridhar, A.; Waldron, G.; Whitebread, S. Reducing safety-related drug attrition: the use of in vitro pharmacological profiling. *Nat. Rev. Drug Discovery* **2012**, *11*, 909−922.
(39) Shultz, M. D.; Cheung, A.; Kirby, C. A.; Firestone, B.; Fan, J.; Chen, Z.; Chin, D. N.; DiPietro, L.; Fazal, A.; Feng, Y.; Fortin, P. D.; Gould, T.; Lagu, B.; Lei, H.; Lenoir, F.; Majumdar, D.; Ochala, E.; Palermo, M. G.; Pham, L.; Pu, M.; Smith, T.; Stams, T.; Tomlinson, R.; Toure, B. B.; Visser, M.; Wang, R.; Waters, N. J.; Shao, W. Identification of NVP-TNKS656: The use of structure efficiency relationships to generate a highly potent, selective and orally active tankyrase inhibitor. *J. Med. Chem.***2013**, DOI: 10.1021/jm400807n.
(40) Cheung, A.; Chin, D. N.; Fan, J.; Shultz, M. D.; Tomlinson, R. 4-Oxo-3,5,7,8-Tetrahydro-4*H*-pyrano{4,3-*d*}pyriminidinyl compounds for use as tankyrase inhibitors. World Patent WO 2013010092 A1, 2013.